

Brief communication: Alternation of thaw zones and deep permafrost in the cold climate conditions of the East Siberian Mountains, Suntar-Khayata Range

Robert Sysolyatin¹, Sergei Serikov¹, Anatoly Kirillin¹, Andrey Litovko¹ and Maxim Sivtsev¹

¹Melnikov Permafrost Institute, Yakutsk, 677000, Russia

Correspondence to: Robert Sysolyatin (robertseesaw@gmail.com)

Abstract. The Suntar-Khayata Range include numerous natural phenomena interacting or depending on permafrost conditions. Here, we examine some patterns of deep permafrost and talik zones on adjacent sites. A 210 m deep borehole in siltstone bedrock was equipped in July 2010 for temperature monitoring of the topmost 15 m and measurements of a deep permafrost temperature profile. The temperature curvature in the upper part has a bend which is consistent with at upper portion justify by climate warming and shows a steady-state linear geothermal profile below 85 m depth with a high geothermal heat flux. A shallow borehole situated at the river floodplain was used to investigate thaw zones temperature regime. Temperatures down to 6.7 m has been monitored at 5-min intervals during heavy rainfall and has had quite peculiar way. The thickness of the season freezing layer reach to 5.7 m, moreover ground temperature increases to 6 °C at 6.7 m depth by groundwater heat transfer. This study provides some new insight on the permafrost condition at one of the coldest places of Northern Hemisphere.

1 Introductions.

The East Siberian Mountains is one of the largest territory of east Siberia, but at the same time is researching how frontier permafrost region. On the other hand, the existing unique environmental conditions and natural cryosphere phenomena (glaciers, aufeis, “Pole of Cold” Oymyakon [located at 63°15'N 143°9'E](#) and Verkhoyansk [located at 67°33'N 133°23'E](#) e.g.) are interesting for the widespread scientific community (Lytkin and Galanin, 2016; Makarieva et al., 2022; Takahashi et al., 2011). Despite the increasing efforts in global permafrost mapping this area has almost no data on direct permafrost measurements and observations, which would be especially relevant in this data-scarce regions.

One of the main permafrost parameter is the permafrost thickness (Osterkamp and Gosink, 1991)_which has considerably importance for paleo-climate reconstruction, hydrogeology description, deposit exploitation etc. The permafrost temperatures profile is controlled by initial surface temperature, bedrock thermal properties and geothermal heat flux (Lachenbruch and Marshall, 1986). Most frequently, the data about deep permafrost is acquired during geological-prospecting works for potential deposits. The expensive costs of deep borehole drilling limit its acquisition facilities, but in our case, we have access to a deep open borehole on gold ore deposit. In a previous study we focused on monitoring the active layer temperature regime by a widespread soil-pit network in an area close-by, but the temperature regime at the layer of zero annual amplitude (ZAA), season freezing layer as well as deep temperatures profiles have never been presented before (Sysolyatin et al., 2020).

~~In a cold climate with MAAT down to -12°C, taliks are almost certain to be avoided~~Thaw zones (taliks) in cold climate conditions with MAAT down to -12°C is extremely rare (Walvoord and Kurylyk, 2016). Since the heat balance of the

36 subarctic is clearly not cold enough to induce talik formation, groundwater processes are more often involved. Taliks
37 formed by thermal waters and open taliks (below large rivers) are well known, but taliks confined to coarse-grained
38 permeable sediments of riverbanks are poorly studied (Makarieva et al., 2019). Floodplain sediments can accumulate
39 water during the warm period and gradually empty in the winter (Mikhailov, 2015). The occurrence of such taliks
40 forms a favorable environment for the growth thermophilic plants out of their species range – e.g., poplar, willow
41 shrub formation.

42 In this brief communication, we present the thermal regime of typical permafrost and talik sites at the Suntar-Khayata
43 Range. The successful embedding of a shallow borehole allows to examine the active layer temperature evolution in
44 a floodplain talik for the first time. We aim to: 1) describe the typical permafrost conditions by possess data and
45 discuss the present temperature changes 2) infer the possible extent of talik zones, discuss the origin of their formation
46 and show the impact of heavy rainfall to ground temperature regime and slope stability. This study presents the general
47 permafrost conditions and discusses possible ways to improve the permafrost mapping of the East Siberian Mountains.

48 **2 Study area.**

49 The Suntar-Khayata Range is located at the southern boundary of the East Siberian Mountains and serves as a
50 watershed between Aldan and Indigirka River basins (Fig. 1). At altitudes between 2000 m asl and 2959 m asl a glacial
51 area is persisting, representing largest of present glaciation in Siberia – with about 195 glaciers cover 163 km²
52 (Ananicheva et al., 2010). The study area is represented by alpine relief with the height of the peaks from 1550 to
53 2031 m asl. The shallow borehole is located at the valley basin of Vostochnaya Khandyga River at 850 m asl (Fig.
54 1d), and the deep borehole is located in the narrow V-shaped valley Vostochnaya Khandyga tributary at 1100 m asl
55 altitude (Fig. 1c). Late Paleozoic sandstone, siltstone and clay slate are prevalent bedrocks of the mountain rock,
56 whereas the valley sediments consist of coarse-grained alluvium strata (Sokolov et al., 2015). ~~Roek glaci~~Kurums
57 ~~are widespread exist~~ at the foot and middle part of the mountain slopes and has widespread distribution (Lytkin and
58 Galanin, 2016)- and boulders can reach up to 3 m in diameter.

59 The climate conditions recorded at a weather station 43 km away from to east of the study site (Vostochnaya,
60 WMO24679), situated at 1288 m asl. The MAAT ranges from -15.3°C to -11.2°C, average precipitation is about 280
61 mm and maximum annual snow thickness vary from the 16 to 60 cm for the 1966-2018 period. Direct air temperature
62 observation around the borehole at the floodplain shown the existence of winter temperature inversion at altitudes
63 between 800 and 1400 m asl (Sysolyatin et al., 2020). The flora is not very diverse. Dwarf Siberian pine is occupying
64 the top part of slopes between 1400 and 1600 m asl and able to accumulate significant snow cover. Siberian larch is
65 growing on gentle and steep slopes, flat surfaces reflecting the most severe permafrost conditions. The poplars have a
66 limited extent, adjacent to the riverbank.

67 According to our soil-pit monitoring network (Sysolyatin et al., 2020), the mean annual ground temperature ranges
68 from -1.1 to -10.6°C at 1 m depth, active layer vary from 0.5 to 2.7 m and mean ground surface temperature can drop
69 to -31°C. No direct observation of precipitation or snow thickness are available for the study area, but its influence is
70 obviously significant. For instance, in 2021 anomalous heavy rains gave rise to numerous debris flows and the
71 appearance of debris avalanches as well as an abrupt change in the talik temperature regime (Supplementary material,
72 Fig. 3).

73 **3 Materials and method**

74 The deep borehole was drilled for prospecting of the orogenic gold deposit prospecting by a geological company in
75 1991. Organic material is almost absent and soil thickness does not exceed 0.5-0.8 m. Core samples (with marked
76 depths interval) were stocked close to the drilling site, where 4 samples have been collected for laboratory studies. In
77 2010 the sintered ice plug in the topmost 5 m was redrilled for establishing a temperature monitoring site. In 2020,
78 temperature measurements were made at intervals of 5 m for depths of 20 to 150 m and 10 m for depths between 150
79 and 210 m using a movable high-precision negative temperature coefficient thermistor and multiconductor cable. To
80 reduce the impact of convection, the hole was plugged by dense material.

81 The shallow borehole was drilled using a wheeled drilling rig in gravel alluvium sediments without core sampling.
82 The hole was cased with a PVC pipe with inner diameter of 20 mm and the sensors were inserted at 1, 3, 5 and 6.7 m
83 depths. The space around the casing was filled by sand and well cutting. The first attempt to drill a borehole in the
84 floodplain was reaching to a depth of 12 m, but a failure of drilling tools halted the process. At end of July the stratum
85 was relatively dry.

86 Ground temperatures were monitored continuously within the shallow and deep borehole down to 6.7 and 15 m for
87 one and 9 years, respectively. Measurements were made every 4 h with TMC50-HD thermistors that were attached to
88 four-channel Onset HOBO data loggers (U12-008 model). Air and ground surface temperatures (2 cm depth) were
89 acquired for the shallow borehole site using a 2-channel data logger (U23-003). The operation design of the different
90 logger systems situated at sites and in interior of the boreholes is shown in Table 1. ~~These logger systems have an~~
91 accuracy of $\pm 0.25^{\circ}\text{C}$ or better and an operation range of -40 to 100°C . Since the sensors installed in the deep borehole
92 at 5 and 15 m, we report the mean annual ground temperature determine the offset of heat wave penetration from
93 surface. In accordance with local climatic conditions and thermal properties of the bedrock, to account for an equal
94 seasonal cycle, MAGT was calculated for the periods September-August and January-December for depths of 5 and
95 15 m, respectively. For the shallow boreholes, the data presented for the high-frequency logging period (every 5 min)
96 from 31 July to 8 September are used trace the impact of heavy rain infiltration events on the subsurface thermal
97 regime.

98 **4 Result**

99 *4.1 Permafrost temperature evolution*

100 At the V-valley site, only two of four sensors (5 and 15 m) have useful and reliable data for analysis (Fig 2a and b).
101 The ground temperatures below 0°C were recorded for the whole monitoring period at 5 m depth. The observed
102 average MAGT is -4.25°C for both depths. The ground temperature evolution show a sinusoidal pattern with smooth
103 drifting following the changing climate condition. At 5- and 15 m depth, the amplitude ranges from 6.2 to 0.6 $^{\circ}\text{C}$,
104 respectively, for the whole measurement period. The fluctuations of mean annual ground temperature did not exceed
105 0.61°C at 5 m and 0.26°C at 15 m. The warming trend that has been highlighted for the 2010 to 2015 period was
106 changing to equivalent cooling until 2019 at both depths. In accordance with the results presented, the ZAA depth
107 might vary from 10.9 to 13.9 for a thermal diffusivity of around $1.21\text{-}1.96 \times 10^{-6} \text{ m}^2 \text{ s}^{-1}$ by core samples. However, as
108 far as the temperature altering should not up over to 0.1°C by annual period, the ZAA layer has been exceed 15 m
109 depth.

110 *4.2 Permafrost thickness and thermal conditions*

111 The permafrost thickness observed by these direct measurements does not exceed 205-210 m in the deep borehole at
112 V-valley. A detailed temperature profile is presented in Fig. 2c. Below the assumed depth of ZAA (20 m), the
113 permafrost temperature increases downwards with a gradient ranging from 0.01 to 0.038 °C⁻¹ m. From the whole
114 temperature curve the mean gradient was calculated as 0.0214 °C⁻¹ m. The initial surface temperature ($T_0 = -5.25$ °C) is
115 obtained by best-fit linear extrapolation from a depth interval of 85-160 m due to the uniform value of the gradient
116 (Lachenbruch and Marshall, 1986). The values for the temperature anomaly (offset value from linear fit) at 20 m (A_{20})
117 and 40 m (A_{40}), were calculated as 0.70 and 0.39 °C, respectively.

118 4.3 Talik temperature regime

119 A simple geomorphology sketch of the shallow borehole site is present in Figure 3a and an annual and monthly
120 temperature-time series for the floodplain site are shown in Figure 3b and c, respectively. The pattern of the 1 m depth
121 temperature evolution is consistent with the air and surface temperature evolution. Temperatures ranged from -6.3 to
122 6.6 °C and from -13.7 to 20.7 °C, respectively. Surprisingly, the temperature variation at 3m depth has been smaller
123 than for the sensors below, just from -2 to 1.6 °C. Refreezing at 3 m depth began at the end of January and the zero-
124 curtain period is present from approximately the end of June to September, dividing the floodplain (overburden)
125 sediments into to 3 zones – upper active layer, intermediate frozen layer and bottom permanent talik. The spike in
126 Figure 3c is related to percolation of warm rainwater to 3 m depth, probably through casing tube. The most peculiar
127 temperature behavior is found for the 5 and 6.7 m depth sensors, which is surely related to heat advection of ground
128 water movement. Patterns of temperature changes at 5 m depth are more linear, whereas at 6.7 m it is more exponential.
129 The maximum absolute temperature ranged between 4.4 °C (5 m) and 7.7 °C (6.7 m), while minimum temperatures
130 oscillated between -0.2 °C (5 m) and 0.3 °C (6.7 m). The ground at a depth of 5 m remained unfrozen for more than
131 75% of the time of the year. In an isopleth plot the [thaw-zonetalik](#) appears below to 5.7 m and obviously continuous
132 downward (Fig 3b). At an air temperature of -9.9 °C and MAGST of -1.8 °C the MAGT for the observation period
133 (almost a year) is -1.1, -0.1, 1.1, 1.8 °C for depths of 1, 3, 5 and 6.7 m, respectively.

134 5 Discussion

135 Permafrost thickness is one of the major components of the cryosphere and has a close relation to geothermal heat
136 flux. According to Balobaev [et al. \(1985\)](#) (~~Balobaev et al., 1985~~) the Suntar-Khayat Range is characterised by high
137 values of geothermal heat flux up to 0.08-0.10 Wm⁻², usually concentrating under narrow V-shaped valleys. Through
138 numerous geothermal measurements at the next orogenic gold deposits (Nezhdaninskoye) specific patterns of thermal
139 conditions were determined. Thus, the angle of inclination of the surface reduces the geothermal heat flux according
140 to the equation:

$$141 \quad q = q_0 \cos \alpha \quad (1)$$

142 where q – calculated geothermal heat flux; q_0 – initial geothermal heat flux, α – slope angle.

143 The interaction between altitude and surface temperature has also been presented in previous studies and might
144 decrease MAGST to -6.5°C at 1800 m asl mountain peaks (Sysolyatin et al., 2020). As mentioned above, MAGT at 5
145 m depth have rather similar value to the ZAA temperature. By the steady-state equation (2) and expect the decrease
146 of the ZAA temperature upon upward height, the permafrost thickness was calculated (Table 1) (Carslow and Jager,
147 1959; Guglielmin et al., 2011). By corn samples, bedrock effective thermal conductivity is 2.41 Wm⁻¹ K⁻¹ and $q_0 =$

148 0.052 Wm⁻² in permafrost body at base altitude surface level – 1100 m According to the orographic configuration of
149 the study area, the permafrost thickness at local peaks 2000 m asl can reach to ~ 500 m.

$$150 \quad Z = T * \frac{\lambda}{q} + ZAA \quad (2)$$

151 where, Z – estimated permafrost thickness, m; T – temperature at the ZAA depth, °C; λ – effective thermal
152 conductivity, Wm⁻¹ °C⁻¹; q – geothermal heat flux in permafrost Wm⁻² (from equation 1).

153 Extrapolation of the linear portion of temperature curve to the surface result in significant differences to the current
154 temperature curve from the initial MAGST features (Lachenbruch and Marshall, 1986). Two variants of changes are
155 considered, a temperature change at the surface and a temperature change at the ZAA. For instance, assuming thermal
156 diffusivity is 1.6×10⁻⁶ m² s⁻¹, the surface temperature shift around 1.4 °C would be ongoing from 22 to 81-year respect
157 to step, linear or exponential way of changes. When the temperature shifts by 0.7°C at the ZAA, the response time
158 will expand to a range of 19 to 90 years. With the available data about the rate of air temperature change at the closest
159 weather station, the second variant is the most plausible. It should be noted that the snow cover can change the surface
160 temperature by more than 5 °C (Gisnas et al., 2014), which is much larger than the air temperature change over the
161 last 80 years (IPCC, 2014).

162 As mentioned above, the talik appearance can only be caused by the thermal influence of superficial or ground water
163 in the cold environments of northeastern Siberia. The absence of permafrost under large rivers and in the areas adjacent
164 to hot springs is well-known. Nevertheless, in our case, where the distance from the main stream exceeds 1 km, the
165 presence of the talik was not assumed before. The reason for the existence of the talik is ambiguous. (⊕) One possibility
166 is the migration of rainwater infiltrating through the "windows" of the ~~rock glaciers~~ skurums on the adjacent slope. The
167 timing of the thermal impact of rainfall is clearly evident on the temperature graph at a depth of 1 m; these spikes have
168 been well explained before (Hinkel et al., 2001). (⊕) The divergent temperature response at depths of 5 and 6.7 m is
169 difficult to explain, perhaps it may be related to the interaction of rainfall with the permafrost occurrence at depth. It
170 could also have been due to a delay in the influence of groundwater supply from the river. However, the response time
171 is largely consistent with the first hypothesis. The influence of groundwater from the river when considering the
172 thawing cycle is certain. On the isopleth plot it is clearly shown that the temperature at the depth of 5 and 6.7 m begins
173 to increase earlier than at a depth of 3 m, which means the proximity to the groundwater is accelerating warming for
174 the coarse-grained sediments. To solve this issue, it would be necessary to install additional piezometric and
175 temperature monitoring sites, as well as to carry out temperature measurements of the river water.

176 The features of floodplain taliks for Kolyma region are considered rather recently (Mikhailov, 2015). It is noted as the
177 crucial reason for the formation of the winter river flow. Floodplain taliks of the region are capable to accumulate
178 huge amounts of water and gradually return it back to the river during low-flow cold season. The main influencing
179 factors are the slope of the river floodplain and the permeability of the sediments. Probably the reason for the
180 appearance of such a large talik is just related to the site-specific conditions of the study area. A sufficiently reliable
181 marker may be the areal of poplar trees, tending to warmer environments. However, in our case, at the drilling site the
182 vegetation was represented by mosses and larch that is more typical for permafrost landscapes.

183 An increase in liquid precipitation, along with increase in air temperature, is one of the most obvious consequences
184 of global warming (Savelieva et al., 2000; Yang et al., 2005). For the permafrost zone, heavy rainfall often acts as a

185 trigger for geomorphological processes (Borgatti and Soldati, 2013). The effect of heavy rainfalls on permafrost is
186 most pronounced for the mountainous areas.

187 The behavior of the upper part of the permafrost during flooding rains, creates reasons for the activation of slope
188 processes. Heavy rains at the end of August 2021 were the trigger for 7 large landslides on a 5 km section of the
189 Kolyma highway, temporarily stopping traffic (Supplementary material). The high concentration of landslides on this
190 section is explained by the aspect and angle of the slope, creating favorable conditions for an increase of the active
191 layer. Abrupt and abundant saturation with rainwater led to critical weighting of soil material, after which the stability
192 of the slope has been disrupted. Landslide processes were also observed everywhere during field investigations in
193 other areas with a lower inclination and northern and eastern aspects. Descriptions of such scenarios are given in many
194 sources, but the detailed process for regions of northeastern Siberia is poorly understood at this time (Frauenfelder et
195 al., 2018; Geertsema et al., 2006; Gruber and Haeberli, 2007).

196 **6 Conclusion**

197 This study provides insight into thermal patterns of permafrost and ~~thaw zones (talik)~~ that can be valuable for future
198 studies of the East Siberian Mountains. Permafrost is almost continuously distributed with a thickness reach to 500
199 m. ~~Thermal properties of the bedrock were obtained through laboratory determinations and a negligible permafrost~~
200 ~~temperature trend was identified as a result of long-term monitoring~~~~By direct measurements and exploration we~~
201 ~~obtained thermal properties and determined the permafrost temperature trend.~~ Due to the successful location of the
202 borehole and high-frequency measurements during rare heavy rains in August 2021, unusually high values of daily
203 precipitation were recorded in the Suntar Khayata Mountains (Verkhoyansk Ridge, Siberia). Due to the abundance of
204 liquid precipitation, peculiarities of the configuration of permafrost and thaw zones, as well as site morphology, the
205 temperature regime of soils has a peculiar feature down to a depth of 6.7 m. The size of the talik zone can be very
206 significant, which must be taken into account in mapping, design and modeling. A wide range of multidisciplinary
207 research is required to improve the understanding of permafrost conditions in this area.

208 *Data availability*

209 The data are available from the authors upon request.

210 *Supplement*

211 Debris landslides evidence are added at ~~supplement~~[Supplement material](#).

212 *Author contributions*

213 ~~RG and SS proposed the initial idea and carried out this study by designing researching sites, analyzing data, and~~
214 ~~organizing and was responsible for the compilation and quality control of the observations. RG, SS, AL and MS~~
215 ~~handled with field works. AK responsible for laboratory determination of rock thermal properties. RG prepared the~~
216 ~~manuscript with contributions from SS, AK, AL and MS.~~

217 *Competing interests*

218 The authors declare that they have no conflict of interest.

219 **Acknowledgments**

220 This study has been funded by Republic of Sakha (Yakutia) and Russian Science Foundation (project N 22-27-20073).
221 The authors acknowledge the Melnikov Permafrost Institute for logistic and field work support. Finally, we thank the
222 reviewer Lutz Schirrmeister, anonymous reviewer, and editor Christian Hauck for comments and suggestions which
223 helped improve the manuscript.

224 **References**

- 225 Ananicheva, M. D., Krenke, A. N. and Barry, R. G.: The Northeast Asia mountain glaciers in the near future by
226 AOGCM scenarios, *Cryosph.*, 4(4), 435–445, doi:10.5194/tc-4-435-2010, 2010.
- 227 Balobaev, V. T., Devyatkin, V. N., Gavriliev, R. I. and Rusakov, V. G.: About geothermophysical researching of
228 mineral deposits at north-east region, *Geol. Geol. Explor.*, 5, 36–37, 1985.
- 229 Borgatti, L. and Soldati, M.: 7.30 Hillslope Processes and Climate Change, in *Treatise on Geomorphology*, pp. 306–
230 319, Elsevier., 2013.
- 231 Carslow, H. S. and Jager, J. C.: *Conduction of Heat in Solids*, Oxford University Press: New York., 1959.
- 232 Frauenfelder, R., Isaksen, K., Lato, M. J. and Noetzli, J.: Ground thermal and geomechanical conditions in a
233 permafrost-affected high-latitude rock avalanche site (Polvartinden, northern Norway), *Cryosph.*, 12(4), 1531–1550,
234 doi:10.5194/tc-12-1531-2018, 2018.
- 235 Geertsema, M., Clague, J. J., Schwab, J. W. and Evans, S. G.: An overview of recent large catastrophic landslides in
236 northern British Columbia, Canada, *Eng. Geol.*, 83(1–3), 120–143, doi:10.1016/j.enggeo.2005.06.028, 2006.
- 237 Gisnas, K., Westermann, S., Schuler, T. V., Litherland, T., Isaksen, K., Boike, J. and Etzelmuller, B.: A statistical
238 approach to represent small-scale variability of permafrost temperatures due to snow cover, *Cryosphere*, 8(6), 2063–
239 2074, doi:10.5194/tc-8-2063-2014, 2014.
- 240 Gruber, S. and Haeberli, W.: Permafrost in steep bedrock slopes and its temperature-related destabilization
241 following climate change, *J. Geophys. Res. Surf.*, 112(F2), doi:10.1029/2006jf000547, 2007.
- 242 Guglielmin, M., Balks, M. R., Adlam, L. S. and Baio, F.: Permafrost Thermal Regime from Two 30-m Deep
243 Boreholes in Southern Victoria Land, Antarctica, *Permafr. Periglac. Process.*, 22(2), 129–139, doi:10.1002/ppp.715,
244 2011.
- 245 Hinkel, K. M., Paetzold, F., Nelson, F. E. and Bockheim, J. G.: Patterns of soil temperature and moisture in the
246 active layer and upper permafrost at Barrow, Alaska: 1993–1999, *Glob. Planet. Change*, 29(3–4), 293–309,
247 doi:10.1016/S0921-8181(01)00096-0, 2001.
- 248 IPCC: *Climate Change 2014*, in *Synthesis Report, Contribution of Working Groups I, II and III to the Fifth*
249 *Assessment Report of the Intergovernmental Panel on Climate Change*, p. 151, Geneva, Switzerland., 2014.
- 250 Lachenbruch, A. H. and Marshall, B. V.: Changing Climate: Geothermal Evidence from Permafrost in the Alaskan
251 Arctic, *Science (80-)*, 234(4777), 689–696, doi:10.1126/science.234.4777.689, 1986.
- 252 Lytkin, V. M. and Galanin, A. A.: Rock glaciers in the Suntar-Khayata Range, *Ice Snow*, 56(4), 511–524,
253 doi:10.15356/2076-6734-2016-4-511-524, 2016.

254 Makarieva, O., Nesterova, N., Post, D. A., Sherstyukov, A. and Lebedeva, L.: Warming temperatures are impacting
255 the hydrometeorological regime of Russian rivers in the zone of continuous permafrost, *Cryosph.*, 13(6), 1635–
256 1659, doi:10.5194/tc-13-1635-2019, 2019.

257 Makarieva, O., Nesterova, N., Shikhov, A., Zemlianskova, A., Luo, D., Ostashov, A. and Alexeev, V.: Giant
258 Aufeis—Unknown Glaciation in North-Eastern Eurasia According to Landsat Images 2013–2019, *Remote Sens.*,
259 14(17), 4248, doi:10.3390/rs14174248, 2022.

260 Mikhailov, V. M.: Geographical regularities of distribution of floodplain taliks, *Izv. Ross. Akad. Nauk. Seriya*
261 *Geogr.*, (1), 65, doi:10.15356/0373-2444-2014-1-65-74, 2015.

262 Osterkamp, T. E. and Gosink, J. P.: Variations in permafrost thickness in response to changes in paleoclimate, *J.*
263 *Geophys. Res. Solid Earth*, 96(B3), 4423–4434, doi:10.1029/90JB02492, 1991.

264 Savelieva, N. ., Semiletov, I. ., Vasilevskaya, L. . and Pugach, S. .: A climate shift in seasonal values of
265 meteorological and hydrological parameters for Northeastern Asia, *Prog. Oceanogr.*, 47(2–4), 279–297,
266 doi:10.1016/S0079-6611(00)00039-2, 2000.

267 Sokolov, S. D., Tuchkova, M. I., Ganelin, A. V., Bondarenko, G. E. and Layer, P.: Tectonics of the South Anyui
268 Suture, Northeastern Asia, *Geotectonics*, 49(1), 3–26, doi:10.1134/S0016852115010057, 2015.

269 Sysolyatin, R., Serikov, S., Zheleznyak, M., Tikhonravova, Y., Skachkov, Y., Zhizhin, V. and Rojina, M.:
270 Temperature monitoring from 2012 to 2019 in central part of Suntar-Khayat Ridge, Russia, *J. Mt. Sci.*, 17(10),
271 2321–2338, doi:10.1007/s11629-020-6175-3, 2020.

272 Takahashi, S., Sugiura, K., Kameda, T., Enomoto, H., Kononov, Y., Ananicheva, M. D. and Kapustin, G.: Response
273 of glaciers in the Suntar–Khayata range, eastern Siberia, to climate change, *Ann. Glaciol.*, 52(58), 185–192,
274 doi:10.3189/172756411797252086, 2011.

275 Walvoord, M. A. and Kurylyk, B. L.: Hydrologic Impacts of Thawing Permafrost-A Review, *Vadose Zo. J.*, 15(6),
276 vzt2016.01.0010, doi:10.2136/vzt2016.01.0010, 2016.

277 Yang, D., Kane, D., Zhang, Z., Legates, D. and Goodison, B.: Bias corrections of long-term (1973-2004) daily
278 precipitation data over the northern regions, *Geophys. Res. Lett.*, 32(19), n/a-n/a, doi:10.1029/2005GL024057,
279 2005.

280

281

282

283

284

285

286

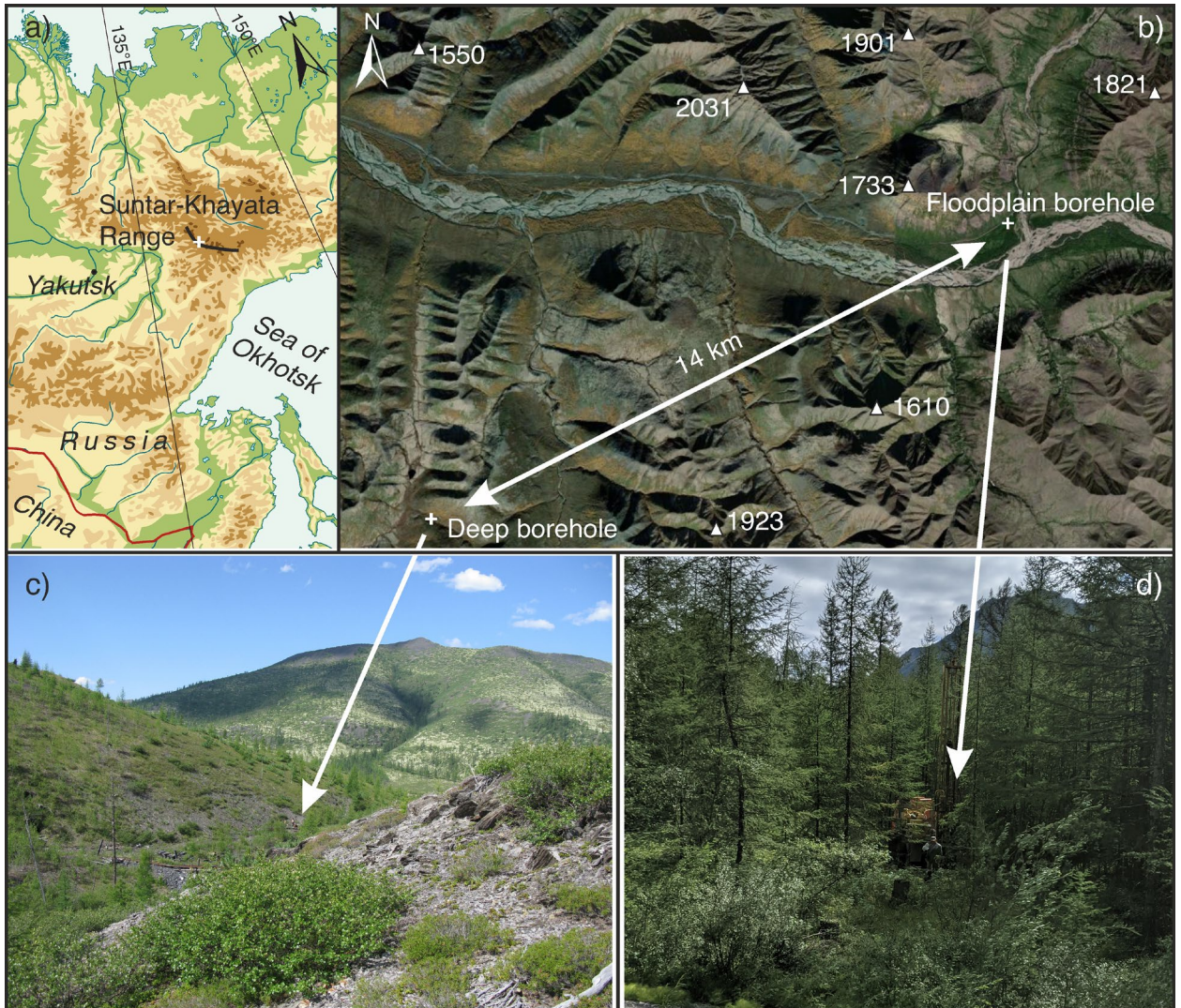
287

288

289

290

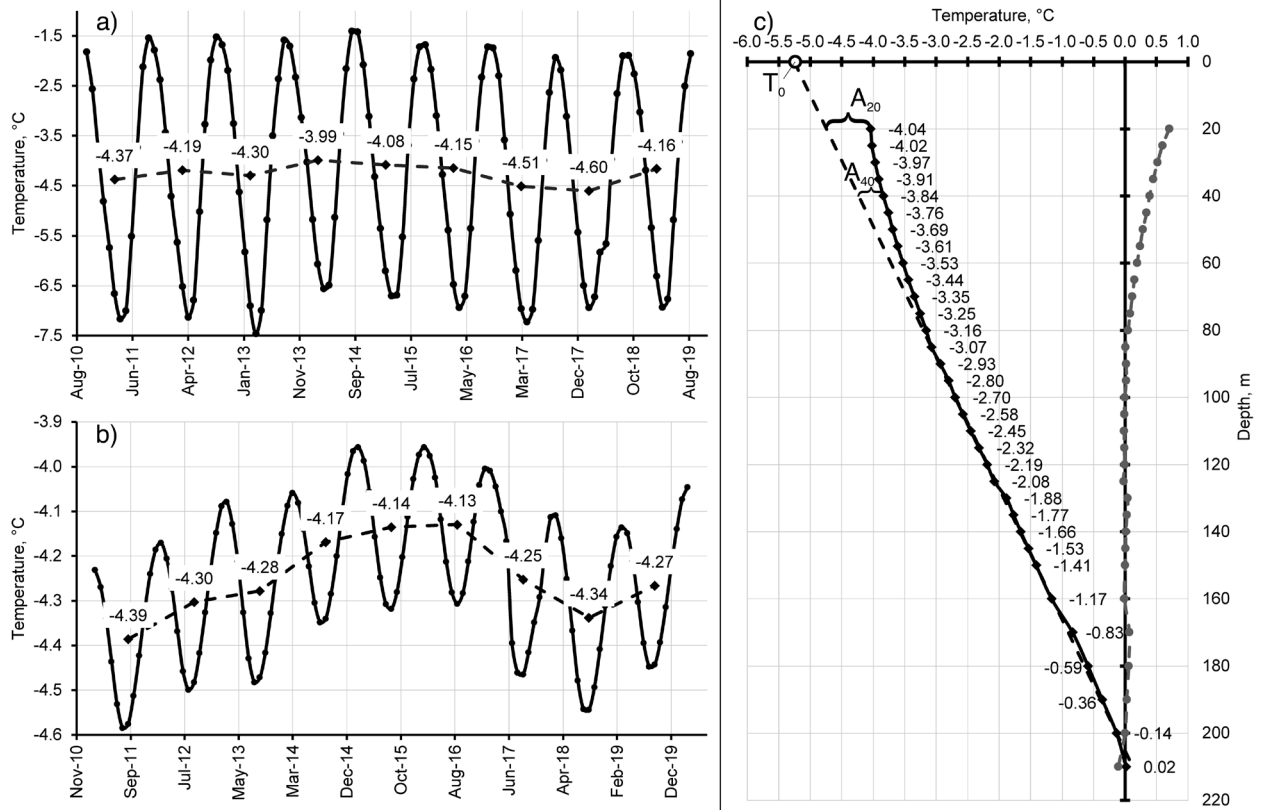
291



292

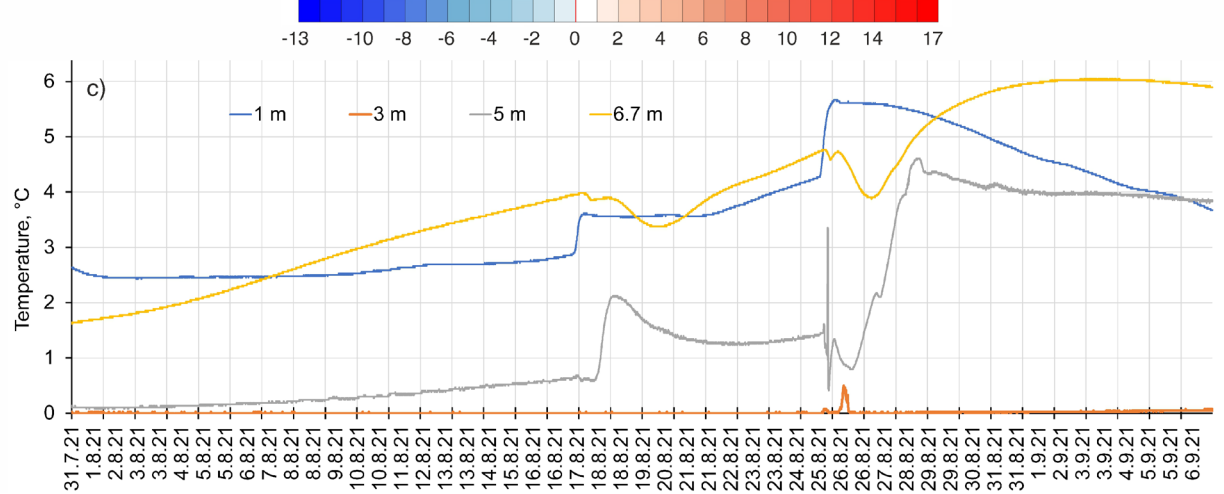
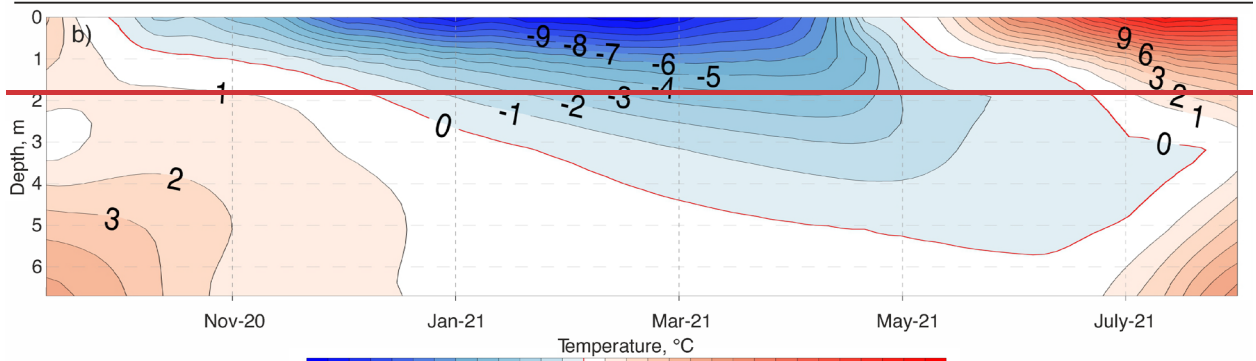
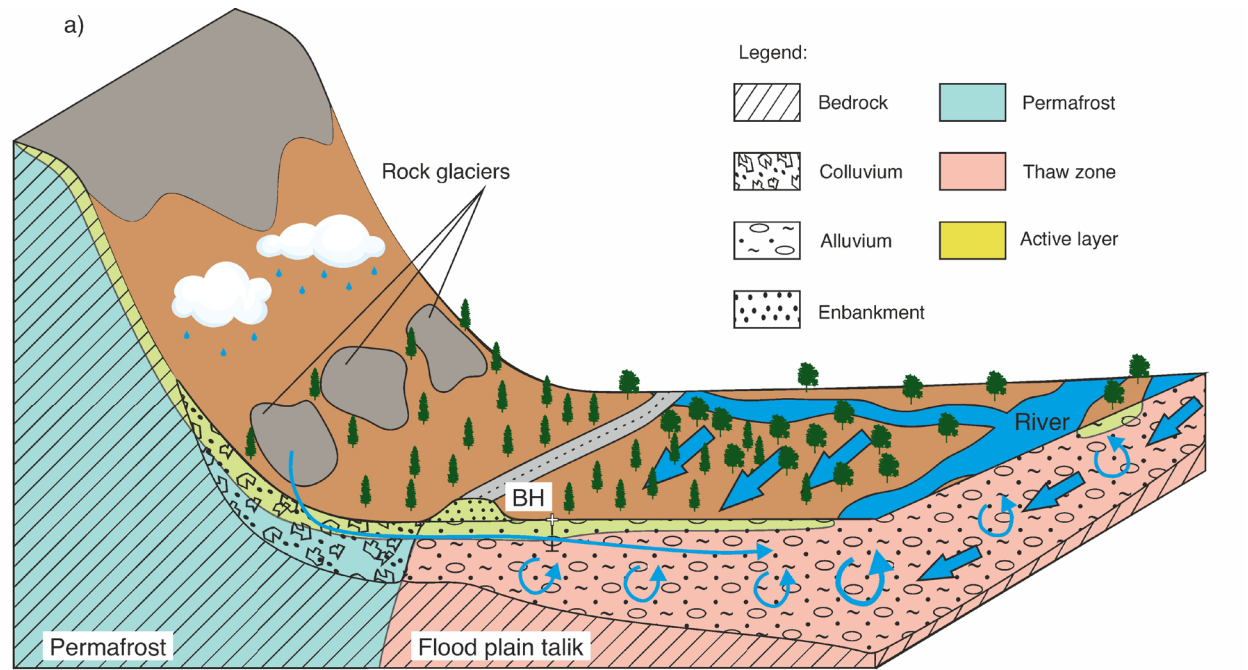
293 **Figure 1. Study area description and picture of sites environment. In (a) a modified physical map of the location of the study**
294 **area in eastern Siberia is shown (Map source: © GEOATLAS 1998). (b) MAXAR image of Vostochnaya Khandyga basin**
295 **with altitudes of peaks. (c) Deep borehole site at V-shaping valley. (d) Shallow borehole site at river plain.**

296

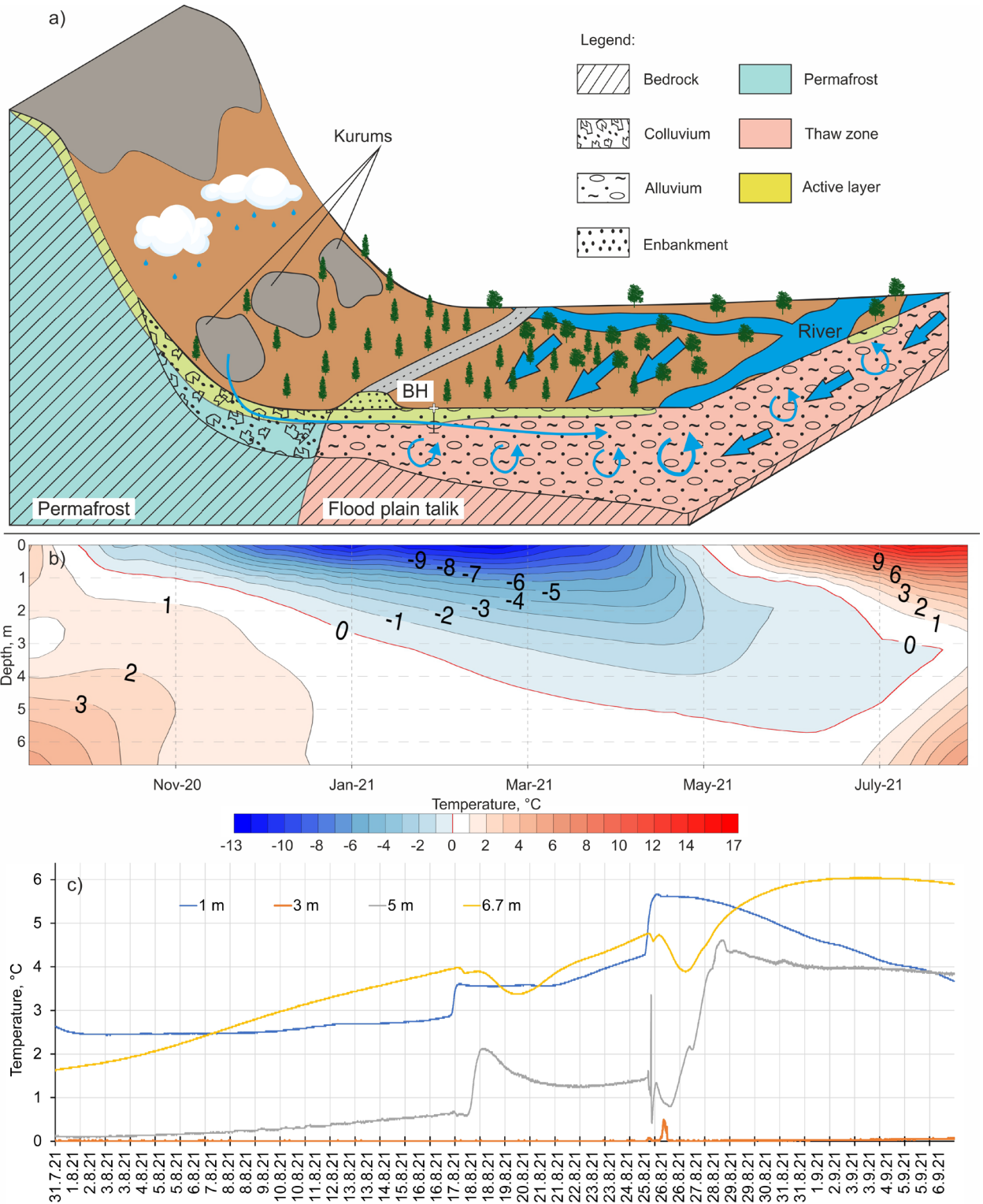


297

298 **Figure 2: Thermal regime of permafrost conditions in the deep borehole. Mean monthly and annual ground temperature**
 299 **evolution at 5 m (a) and 15 m (b) depth. (c) Temperature profile (solid line), best linear-fit (dashed line) and current offset**
 300 **from extrapolated temperature (dotted line).**



301



302

303

304

Figure 3: (a) The scenario of ground water flow of the floodplain talik. (b) Annual ground temperature evolution and (c) temperature fluctuation at a heavy rain event.

305

306

307

308

309

Table 1

310

311

General parameters of equipment and operating timing of the loggers installed at different depths inside the boreholes during the control period.

<u>Location</u>	<u>Logger system and sensor</u>	<u>Accuracy and operation range</u>	<u>Sensor's depth, m</u>	<u>Measuring interval and operating time</u>
<u>River flood plain, Shallow borehole</u>	<u>OnSet Hobo U12-008</u>	<u>±0.25 °C at range -40 to 100 °C</u>	<u>1, 3, 5, 6.7</u>	<u>Every 5 min from 31-Jul-2021 to 7-Sep-2021/</u> <u>Every 4 h from 8-Sep-2021 to 18-Aug-2022</u>
<u>River flood plain, Shallow borehole</u>	<u>OnSet Hobo U23-003</u>		<u>Air, Surface</u>	
<u>V-shaped valley, Deep borehole</u>	<u>OnSet Hobo U12-008</u>		<u>1*, 5, 10**, 15</u>	<u>Every 4 h from 20-Jul-2010 to 9-Sep-2021</u>

312

*non valid cause to close position to borehole's iron case tube

313

**non valid because of misgiving temperature data at long period

314

315

Table 1

316

Permafrost thickness based on the assumption that MAGT and permafrost heat flow are decreasing under step-up of peaks height.

317

Peak altitude, m	Slope inclination (α), grad	Cos α	Temperature at ZAA (20 m depth), °C	q, Wm ⁻² ,	Permafrost thickness, m
1550	24.2	0.912	-5.5	0.047	298
1600	26.6	0.894	-5.7	0.047	314
1700	31.0	0.857	-6.0	0.045	343
1800	35.0	0.819	-6.5	0.043	386
1900	38.7	0.781	-7.0	0.041	434
2000	42.0	0.743	-7.5	0.039	486

318